

# Tomography of stellar halos: what does anisotropy in a stellar halo tell us?

Biswajit Pandey<sup>a</sup>

<sup>a</sup>Department of Physics, Visva-Bharati University, Santiniketan, 731235, India

E-mail: [biswap@visva-bharati.ac.in](mailto:biswap@visva-bharati.ac.in)

**Abstract.** The stellar halo of the Milky Way is known to have a highly lumpy structure due to the presence of tidal debris and streams accreted from the satellite galaxies. The abundance and distribution of these substructures can provide a wealth of information on the assembly history of the Milky Way. We use some information-theoretic measures to study the anisotropy in a set of Milky Way-sized stellar halos from the Bullock & Johnston suite of simulations that uses a hybrid approach coupling semi-analytic and N-body techniques. Our analysis shows that the whole-sky anisotropy in each stellar halo increases with the distance from its centre and eventually plateaus out beyond a certain radius. All the stellar halos have a very smooth structure within a radius of  $\sim 50$  kpc and a highly anisotropic structure in the outskirts. At a given radius, the anisotropies at a fixed polar or azimuthal angle have two distinct components: (i) an approximately isotropic component and (ii) a component with large density fluctuations on small spatial scales. We remove the contributions of the substructures and any non-spherical shape of the halo by randomizing the polar and azimuthal coordinates of the stellar particles while keeping their radial distances fixed. We observe that the fluctuating part of the anisotropy is completely eliminated, and the approximately uniform component of the anisotropy is significantly reduced after the sphericalization. A comparison between the original halos and their sphericalized versions reveals that the approximately uniform part of the anisotropy originates from the discreteness noise and the non-spherical shape of the halo whereas the substructures contribute to the fluctuating part. We show that such distinction between the anisotropies has the potential to constrain the shape of the stellar halo and its substructures.

---

## Contents

<b>1</b>	<b>Introduction</b>	<b>1</b>
<b>2</b>	<b>Data and method of analysis</b>	<b>4</b>
2.1	Stellar halo catalogue	4
2.2	Sphericalized halos	5
2.3	Mock halos with different shapes	5
2.4	Information entropy based anisotropy measures	5
2.4.1	Whole-sky anisotropy within a given radius	5
2.4.2	Anisotropy at fixed polar angle within a given radius	7
2.4.3	Anisotropy at a fixed azimuthal angle within a given radius	7
<b>3</b>	<b>Results</b>	<b>7</b>
3.1	Effects of binning on the anisotropy	7
3.2	Comparison with sphericalized halos: shape versus substructures	11
3.3	Comparison of anisotropy in different stellar halos	12
<b>4</b>	<b>Conclusions</b>	<b>12</b>

---

## 1 Introduction

Understanding the formation and the evolution of galaxies remains one of the most interesting and challenging problems in cosmology. We do not yet completely understand the details of galaxy formation despite the many successes of the  $\Lambda$ CDM model on large scales. In the current paradigm, the galaxies form at the centre of the dark matter halos via cooling and condensation of baryons [1]. The galaxies grow further by accretion of matter and mergers with other galaxies. In the hierarchical clustering scenario [2, 3], the larger structures are formed via the merger of smaller structures, leading to even larger structures like clusters and superclusters in the Universe. However, it is essential to test the hierarchical growth of structures on the scales of galaxies to understand their origin and evolution.

The Milky Way is believed to have formed via a series of mergers with other galaxies. Our galaxy has several distinct components: the thin and thick disk, the bulge, the bar, and a diffuse stellar halo. The stellar halo, a quasi-spherical distribution of stars, envelops the disk and the bulge and extends to a few hundreds of kpc. It contains  $\sim 1\%$  of the total stars in the Milky Way. The structure of the stellar halo is intimately linked to the formation of our galaxy [4]. In the case of hierarchical growth, a significant fraction of the stellar halo is expected to have formed from the accreted and disrupted satellite galaxies [5–10]. Consequently, the stellar halo would serve as a repository of merger debris and contain the fossil evidence of the accretion and merger events that led to the formation of the galaxy. A detailed review of the Milky Way’s stellar halo can be found in [11].

The classic paper by Eggen et al. (1962) [12] analyze the proper motions and radial velocities of 221 dwarf stars in the stellar halo and find that the stars with lower metallicity tend to move in highly eccentric orbits. They interpret this correlation as a consequence of the formation of the metal-deficient stars in a rapid collapse of a spherical cloud in the radial direction. Contrary to this, Searle & Zinn (1978) [13] find a wide range of metallicities in

a sample of 19 globular clusters located at different galactocentric distances. Their analysis suggests a gradual agglomeration of the stellar halo from the accretion of many dwarf satellites. Subsequently, many observational studies are carried out to understand the formation of the Milky Way and its stellar halo [14–30, 69]. Nevertheless, whether the stars in the stellar halo form in situ in the early phases of the collapse of the Milky Way or form in satellite galaxies that were accreted by the Milky Way at a later stage is still a matter of debate. The two scenarios can be tested by studying the structure of the stellar halo [32]. The actual process may be a combination of these two pictures [33]. The stellar halo is expected to have ellipsoidal symmetry and devoid of substructure if the halo stars form in situ via the radial collapse of a protogalactic cloud many dynamical times ago. On the other hand, a significant fraction of the stellar halo would be made up of accumulated debris if the halo stars are accreted from the satellite galaxies. The accreted debris from the disrupted satellite galaxies would gradually disperse in real space. The stellar halo may appear smooth despite undergoing many episodes of accretion. Nonetheless, debris accreted in the last few gigayears can remain spatially coherent [7, 8]. Further, some information about the initial conditions can still be recovered from the phase space distribution of the stars [34].

The identifications of the substructures and their distributions inside the stellar halo can unravel the assembly history of the Milky Way. So, despite its low luminosity and density, the stellar halo can provide important constraints on scenarios for the formation and evolution of the Galaxy. Several substructures have been identified in the stellar halo of the Milky Way in the last few decades. The Orphan Stream [35–37], the Sagittarius dwarf tidal stream [14, 38, 39], the low-latitude stream [40, 41], the Virgo, Hercules–Aquila and Pisces overdensities [18, 42–44] are some of the prominent substructures observed in the stellar halo of the Milky Way. Moreover, the existence of substructures is also confirmed in the stellar halo of M31 [45–49], M33 [48, 49] and in other nearby spirals [50–52]. These observations indicate that accretion from satellite galaxies definitely has some role in building the stellar halo of a galaxy.

We also require a theoretical understanding of the formation of stellar halos in a cosmological context. Significant efforts have been made in this direction in the last two decades [7–9, 53, 54]. Bullock & Johnston (2005) [8] study the formation of stellar halos using a semi-analytic approach coupled with N-body that follows accretion of satellite galaxies onto Milky Way-sized halos with an analytic, time-dependent rigid potential. The analytic potential in such model includes terms for both a dark matter halo and a central baryonic disk. Cooper et al. (2010) [9] follow the growth of stellar halos by combining semi-analytic galaxy formation model (GALFORM) with cosmological dark matter simulations from the Aquarius project [55]. More recently, several high-resolution hydrodynamical simulations, such as Auriga [56] and Artemis [57], have modelled the assembly of Milky Way-like stellar halos. An important distinction between the Bullock & Johnston simulation and these simulations is that they are dynamically self-consistent. The model stellar halos derived from these simulations allow one to make quantitative predictions for the density profile, degree of substructure and the properties of the stellar content in the halo.

The distributions of stars in the stellar halo can be highly anisotropic due to the presence of the remnant stellar streams and debris. The word ‘anisotropy’ in the present work refers to the deviations from an isotropic density distribution, measured over cells projected on the sky. Previously, counts-in-cells measures have been used to study the substructure-induced non-uniformity in stellar halos [16, 58]. The variance of the count in cells in such studies can be useful measure of non-uniformity. However, we define our anisotropy measures based on

the information entropy [78]. The information entropy was originally introduced by Claude Shannon in his 1948 seminal paper "A Mathematical Theory of Communication" [78]. It was proposed to quantify the information loss during communication through noisy channels. The Shannon entropy  $H(X)$  for any discrete random variable  $X$  with  $n$  outcomes  $\{x_i : i = 1, \dots, n\}$  is defined as,

$$H(X) = - \sum_{i=1}^n p(x_i) \log p(x_i) \quad (1.1)$$

where  $p(x_i)$  is the probability of the  $i^{\text{th}}$  outcome and  $-\log p(x_i)$  is the information contained in the  $i^{\text{th}}$  outcome of the random variable  $X$ . The negative sign ensures that the information is always positive or zero. A certain event with a probability of 1 would contain no information. Rare events with smaller probability are more uncertain and contain more information. Thus, the information entropy  $H(X)$  is the average information required to describe the random variable  $X$ . In other words, it characterizes the uncertainty in the random variable.

We use the information entropy to define a set of anisotropy measures that can quantify the variation between the counts in cells across patches of a given solid angle on the sky. A randomly chosen star can reside in only one of these cells. So there are as many possible outcomes of the event as the total number of cells. The probability of finding the aforementioned star in a given cell can be determined from the star count in it. This probability can be used to define an anisotropy measure by combining the information entropy and its maximum value. A set of such anisotropy measures can be constructed, following different strategy for grouping the cells. One can study the variation in the cells across the entire sky or restrict the analysis to cells in a given range of polar or azimuthal angle. The anisotropy measure can be either a function of the radial co-ordinate or a combination of radial, polar and azimuthal co-ordinates based on the strategy adopted for grouping the cells.

Our choice for the information entropy based measures over the conventional measures like variance is based on the fact that the information entropy is related to the higher-order moments of a probability distribution [79]. Hence it can contain more information about the distribution.

The anisotropy in the stellar halo may contain important information about its formation. The debris from the earliest merger events is expected to be concentrated at the center of the halo, where the dynamical time is shorter, thus to be more thoroughly mixed in phase space. A study of the radial variation of the full sky anisotropy in the distribution of stars can verify this paradigm. The density profile of the stellar halo is known to roughly scale as  $r^{-3}$  in the inner region, and a steeper variation is observed in the outer parts [16, 20, 24]. The shape of the stellar halo can also provide useful information about its formation. The deviations of the halo shape from the spherical symmetry may have multiple origin. The large-scale departure from spherical symmetry may arise due to contributions from a disk-like component [10, 59, 60, 70], dominant merger events [27, 61, 64–67], violent relaxation [62, 63] or filamentary accretion [71, 72]. On the other hand, the small-scale anisotropy in a stellar halo is primarily caused by coherent substructures [16, 68, 69].

We intend to analyze the anisotropies in the simulated stellar halos to infer useful information about the distribution of the substructures and the shape of the halo. We would like to clarify here that throughout this work, both the diffuse streams or clouds and the bound satellites are considered as substructures. Pandey (2016) [73] propose a method for quantifying the anisotropy in a three-dimensional distribution using information entropy. Subsequently, the method has been used to test the isotropy in the galaxy distribution in the 2MASS and

SDSS [74, 76]. Pandey (2017) [75] show that the method can also be used to determine the linear bias parameter which describes the relationship between the galaxy distribution and the cosmic mass density field. Here, by applying the same technique, we obtain anisotropy profiles for the simulated stellar halos, measured over the whole sky and in bins of azimuthal and polar angle. We use these to investigate the connection between potentially observable anisotropy signals and the formation history of stellar halos. We examine the separate contributions to the anisotropy from substructures and large-scale variations in shape. Our results provide a theoretical foundation for future applications of this technique to data from surveys of the real Milky Way halo.

The paper is organised as follows. We describe the data and the method of analysis in Section 2, discuss the results in Section 3 and present our conclusions in section 4.

## 2 Data and method of analysis

### 2.1 Stellar halo catalogue

Bullock & Johnston (2005) [8] use a semi-analytic formalism combined with a N-body approach to follow the dynamical evolution of the accreted satellite galaxies and provide the accretion histories for 11 Milky Way-sized halos. They assume a  $\Lambda$ CDM framework with  $\Omega_m = 0.3$ ,  $\Omega_\Lambda = 0.7$ ,  $\Omega_b h^2 = 0.024$ ,  $h = 0.7$  and  $\sigma_8 = 0.9$ . We use the 11 stellar halos from the Bullock & Johnston (2005) suite of simulations for our analysis.

We want to calculate the anisotropies in the distribution of stars in these halos in the radial, polar and azimuthal directions.

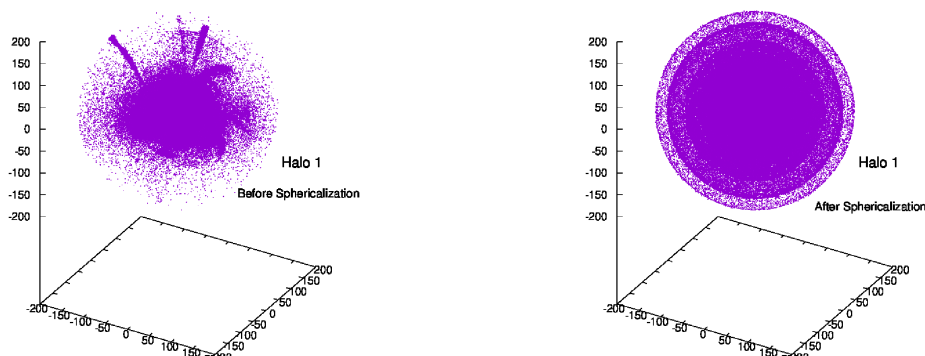


**Figure 1.** The left panel of this figure shows the distribution of the stellar particles within a radius of 200 kpc. The right panel shows the same after the polar and the azimuthal coordinates of all the stellar particles are randomized while keeping their radial coordinates fixed.

## 2.2 Sphericalized halos

The stellar halos are known to be highly lumpy due to the presence of substructures. Lumpiness in a stellar halo is expected to introduce larger values of the anisotropy parameter. The non-spherical shape of the stellar halo may also contribute to the measured anisotropy. We want to quantify the anisotropies induced by the shape of the stellar halo and the substructures within it. It would be interesting if the contributions from the shape and substructures can be separated. It would allow us to constrain the shape and substructures of a halo. To investigate this possibility, we randomly extract one million stellar particles within a radius of 200 kpc from the centre of each stellar halo. We prepare 10 such randomly extracted versions for each stellar halo. In each such halo, we then randomize the polar and azimuthal coordinates  $(\theta, \phi)$  of all the stellar particles without changing their radial coordinates  $r$  (Figure 1). This randomization of the  $(\theta, \phi)$  coordinates would destroy all the substructures present within the original stellar halo. Additionally, it would also obliterate all the information about the shape of the stellar halo. It may be noted that the radial density profile of the original stellar halo would remain intact after the sphericalization. We estimate the  $1 - \sigma$  errorbars for the anisotropy from the 10 sub-samples drawn from each stellar halo.

## 2.3 Mock halos with different shapes

We also generate smooth distribution of particles within non-spherical regions using the Monte Carlo technique. We consider the following three shapes for the mock stellar halos: (i) oblate spheroid ( $a = 1, b = 1, c = 0.75$ ), (ii) prolate spheroid ( $a = 1, b = 1, c = 1.5$ ) and (iii) triaxial ellipsoid ( $a = 1.5, b = 0.88, c = 0.75$ ). In each type of distribution, one million particles are distributed within a volume comparable to the volume of the randomly extracted versions ( $R = 200$  kpc) of the original halo. The density distribution in each halo follows a power law of the form  $r^{-3}$ . We simulate 10 mock stellar halos for each shape. We use these mock halos to calculate the anisotropies introduced by the shape of the stellar halo. Here, we would like to mention that the principal axes of the non-spherical halos coincide with the coordinate axes. One can also consider non-spherical halos with different orientations. We do not consider such halos in this work for simplicity. It is worthwhile to mention here that the coordinate system of the Bullock & Johnston model is oriented such that the  $z$  axis is aligned along the minor axis of the disk potential.

## 2.4 Information entropy based anisotropy measures

### 2.4.1 Whole-sky anisotropy within a given radius

We use the information theoretic definition of anisotropy proposed in Pandey (2016) [73] to study the anisotropy in a stellar halo. We would like to study the anisotropy in the distribution of stars with respect to an observer located at the centre of the halo. We first divide the  $4\pi$  steradian solid angle around the central observer into a number of solid angle bins of equal size. This is achieved by binning  $\cos\theta$  and  $\phi$  into  $m_\theta$  and  $m_\phi$  bins respectively. This results into a total  $m_{total} = m_\theta m_\phi$  solid angle bins of equal size  $d\Omega = \sin\theta d\theta d\phi$ . Each of these solid angle bins would cover exactly the same volume  $dv = \frac{r^3}{3} d\Omega$  within a given radius  $r$  from the centre of the halo. The whole sphere has a solid angle of  $4\pi$  steradian which is  $\sim 41253$  square degree. The solid angle or the area corresponding to each bin can be simply obtained by dividing these numbers by  $m_{total}$ . Each bin covers exactly same area on the sky. The radius  $r$  can be varied within a range  $0 < r \leq r_{max}$ .

We define a random variable  $X_{\theta\phi}$  as the event of finding a star within a distance  $r$  from the centre of the halo. There are a total  $m_{total}$  volume elements around the central observer and a randomly chosen star can occupy any one of these volume elements. So there are  $m_{total}$  probable outcomes for this event. The probability of the  $i^{th}$  outcome is given by,  $f_i = \frac{n_i}{\sum_{i=1}^{m_{total}} n_i}$  with the constraint  $\sum_{i=1}^{m_{total}} f_i = 1$ . Here,  $n_i$  is the number count of stars in the  $i^{th}$  volume element within a given radius  $r$ .

The information entropy associated with the random variable  $X_{\theta\phi}$  can be expressed as,

$$\begin{aligned} H_{\theta\phi}(r) &= - \sum_{i=1}^{m_{total}} f_i \log f_i \\ &= \log N - \frac{\sum_{i=1}^{m_{total}} n_i \log n_i}{N} \end{aligned} \quad (2.1)$$

where  $N$  is the total number of stars within radius  $r$ . The base of the logarithm can be chosen arbitrarily and we choose it to be 10.

If we consider an isotropic distribution of stars in the halo then each of the  $m_{total}$  volume element would contain nearly the same number of stars within them. The probability  $f_i$  for each of the  $m_{total}$  volume element would be same for such a distribution. This maximizes the uncertainty in  $X_{\theta\phi}$  since each of the volume element hosts the same number of stars. The maximum information entropy for a given choice of  $m_\theta$ ,  $m_\phi$  and  $r$  is  $(H_{\theta\phi})_{max} = \log m_{total}$ . We define the whole-sky anisotropy parameter within a given radius  $r$  as  $a_{\theta\phi}(r) = 1 - \frac{H_{\theta\phi}(r)}{(H_{\theta\phi})_{max}}$ . Ideally one would expect  $H_{\theta\phi} = \log m_{total}$  or  $a_{\theta\phi} = 0$  for an isotropic distribution. However, a fluctuations in the number counts would be present at smaller radii due to the Poisson noise. Such fluctuation due to the Poisson noise is expected to diminish with increasing number counts at larger radii. However, the anisotropy parameter would never become exactly zero for even an isotropic distribution due to the finite number of particles and volume. A distribution can be regarded as isotropic provided the observed anisotropies are consistent with the expected Poisson noise at the same sampling rate and choice of binning.

The stellar halos are known to host a wealth of substructures. The presence of these substructures is expected to introduce large fluctuations in the star counts across the  $m_{total}$  volume elements. Any deviation from sphericity of the halo is also expected to introduce significant fluctuations in the number count of stars. The fluctuations in the star counts would decrease the uncertainty in  $X_{\theta\phi}$  by reducing the information entropy  $H_{\theta\phi}$  associated with it. The anisotropy parameter  $a_{\theta\phi}$  would be higher for greater reduction in the information entropy. The anisotropy  $a_{\theta\phi}$  would reach its maximum value 1 for a distribution where all the stars occupy a single volume element without any uncertainty ( $H_{\theta\phi} = 0$ ) in their locations. This extreme situation corresponds to the maximum anisotropy in the distribution.

One can study the whole-sky anisotropy parameter  $a_{\theta\phi}(r)$  by progressively probing a larger distance ( $r$ ) from the centre of the halo. The radial distance limit is increased in steps from a small radius  $r$  to a maximum radius  $r_{max}$  for a given choice of  $m_\theta$  and  $m_\phi$ . Here we would like to mention that  $a_{\theta\phi}(r)$  can be also calculated in a series of independent radial bins.

The  $a_{\theta\phi}(r)$  is expected to steadily decrease with  $r$  for a homogeneous, isotropic random distribution of stars. We use  $a_{\theta\phi}(r)$  to study the radial variation of the whole-sky anisotropy in a stellar halo.

### 2.4.2 Anisotropy at fixed polar angle within a given radius

One can define the anisotropy at fixed polar angle for a given choice of  $m_\theta$ ,  $m_\phi$  and  $r_{max}$  in a similar manner. The information entropy for a fixed radius  $r$  and a given  $\theta$  can be written as,

$$\begin{aligned} H_\phi(\theta) &= - \sum_{i=1}^{m_\phi} f_i \log f_i \\ &= \log N_\theta - \frac{\sum_{i=1}^{m_\phi} n_i \log n_i}{N_\theta} \end{aligned} \quad (2.2)$$

Here  $N_\theta = \sum_{i=1}^{m_\phi} n_i$  is the total number of stars lying in the  $m_\phi$  volume elements within a radial distance  $r_{max}$  at any given  $\theta$ . We define  $f_i = \frac{n_i}{N_\theta}$  in Equation 2.2 where the sum is carried out over all the  $\phi$  bins.

We define the anisotropy parameter at fixed polar angle  $a_\phi(\theta) = 1 - \frac{H_\phi(\theta)}{(H_\phi)_{max}}$  where  $(H_\phi)_{max} = \log m_\phi$ . For a fixed radial distance limit  $r_{max} = R$ , we measure the anisotropy parameter  $a_\phi(\theta)$  at different values of  $\theta$ . This measures the anisotropy in the polar direction by considering all the  $\phi$  bins at each  $\theta$ .

### 2.4.3 Anisotropy at a fixed azimuthal angle within a given radius

Similarly, we define the anisotropy at fixed azimuthal angle for a given choice of  $m_\theta$ ,  $m_\phi$  and  $r_{max}$ . The information entropy for a fixed radius  $r$  and a given  $\phi$  is obtained by carrying out the sum across all the  $\theta$  bins and is defined as,

$$\begin{aligned} H_\theta(\phi) &= - \sum_{i=1}^{m_\theta} f_i \log f_i \\ &= \log N_\phi - \frac{\sum_{i=1}^{m_\theta} n_i \log n_i}{N_\phi} \end{aligned} \quad (2.3)$$

Here  $N_\phi = \sum_{i=1}^{m_\theta} n_i$  is the total number of stars lying in the  $m_\theta$  volume elements within a given  $r_{max}$  at a given  $\phi$ . We have  $f_i = \frac{n_i}{N_\phi}$  and the sum is carried out over all the  $\theta$  bins in the Equation 2.3.

We define the anisotropy parameter at fixed azimuthal angle  $a_\theta(\phi) = 1 - \frac{H_\theta(\phi)}{(H_\theta)_{max}}$  where  $(H_\theta)_{max} = \log m_\theta$ . We determine the anisotropy parameter  $a_\theta(\phi)$  for different values of  $\phi$  while keeping the radial distance limit  $r_{max} = R$  fixed. The parameter  $a_\theta(\phi)$  thus measures the anisotropy in the azimuthal direction by considering all the  $\theta$  bins at each  $\phi$ .

It may be noted that both  $a_\phi(\theta)$  and  $a_\theta(\phi)$  can be measured for different limiting radius and hence can be also written as,  $a_\phi(\theta, r)$  and  $a_\theta(\phi, r)$  respectively.

All three anisotropy parameters defined here probe the structure of the stellar halo and complement each other.

## 3 Results

### 3.1 Effects of binning on the anisotropy

The information entropy is known to be sensitive to the choice of bins. Naturally, the anisotropy measures based on the information entropy would be also sensitive to the binning

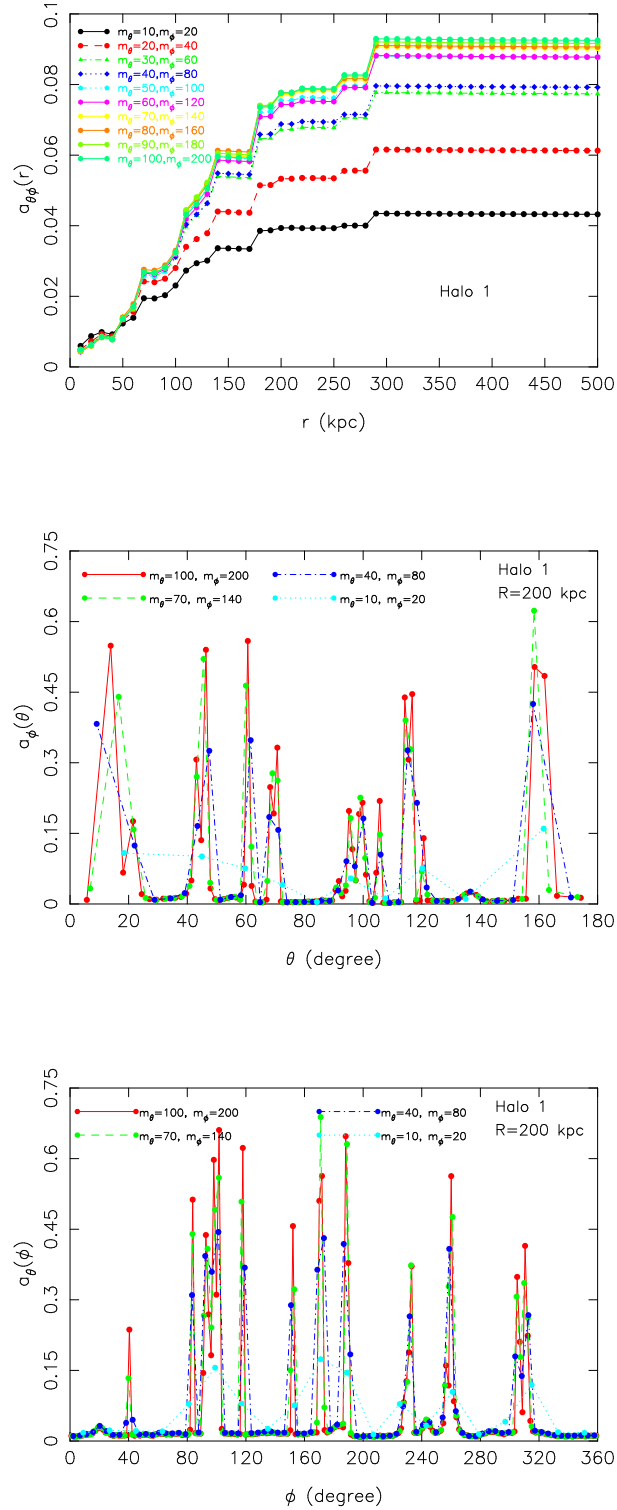


**Figure 2.** The top, middle and bottom panels of this figure respectively show the whole-sky anisotropy, the anisotropy at fixed polar angle and anisotropy at fixed azimuthal angle in Halo 1 for different choices of number of bins.

adopted in the analysis. However, this does not pose any problem provided we understand the effects of binning on the anisotropy and any comparisons of anisotropy are carried out with precisely the same number of bins.

In this subsection, we first address the effects of bin size in the measurement of anisotropies in the stellar halo. In [Figure 2](#), we show the different anisotropies in one of the stellar halos (Halo 1) for different choices of  $m_\theta$  and  $m_\phi$ .

The top panel of [Figure 2](#) shows the whole-sky anisotropy in the Halo 1 as a function of the distance  $r$  from the centre of the halo. The results are shown for 10 different choices of bin size. We find that the anisotropy in the stellar halo increases with the distance from the centre of the halo. The anisotropy keeps increasing up to a radius of  $\sim 270$  kpc beyond which it plateaus to a constant value. A larger  $m_{total}$  corresponds to smaller size of the solid angle bins. The volume covered by each solid angle bin at a distance  $r$  would decrease with increasing  $m_{total}$ . So the larger values of  $m_\theta$  and  $m_\phi$  would result into smaller volume elements giving rise to a larger fluctuations in the star counts. At any given radius  $r$ , a larger degree of anisotropy is expected for a larger  $m_{total}$ . Such differences are caused by (i) presence of lumps and tidal streams on smaller scales and (ii) increase in the Poisson noise due to the smaller number counts. A smaller  $m_{total}$  would probe larger volume elements, thereby decreasing the Poisson noise. It would also decrease the disparity in the abundance of lumps and streams across the different elemental volumes. So the observed anisotropy at any given radius  $r$  should decline with the decreasing number of solid angle bins ( $m_{total}$ ). Interestingly, we find that the stellar halo exhibit a minimal degree of anisotropy within a radius of  $\sim 50$  kpc. The observed anisotropies within 50 kpc for the different choices of  $m_\theta$  and  $m_\phi$  are nearly indistinguishable. This suggests that the core of the halo has a very smooth structure with little to no substructures. The finite anisotropy at the core of the halo may arise due to the discreteness noise and its anisotropic shape at these radii. The gradual increase in the anisotropy  $a_{\theta\phi}(r)$  beyond 50 kpc indicates that the abundance of substructures and anisotropy in their distribution increase with the radial distance from the centre of the halo. The variation of anisotropy ceases beyond  $\sim 270$  kpc indicates the absence of substructures beyond this radius. All the different choices of  $m_\theta$  and  $m_\phi$  reveal the same trend in the variation of  $a_{\theta\phi}(r)$ . We also note that whole-sky anisotropy  $a_{\theta\phi}(r)$  tends to converge at higher values of  $m_{total}$ .

We show the anisotropy at fixed polar angle  $a_\phi(\theta)$  as a function of  $\theta$  and the anisotropy at fixed azimuthal angle  $a_\theta(\phi)$  as a function of  $\phi$  in the middle and bottom panels of [Figure 2](#) respectively. In both cases, we fix the radial distance limit  $r_{max}$  to 200 kpc and show the results for only four different choices of bins for clarity. The two anisotropy profiles of the Halo 1 show a number of distinct spikes. These spikes indicate a sudden rise in the anisotropy in the halo along certain polar and azimuthal directions. The anisotropy at the spikes are significantly larger compared to the remaining directions. These spikes in the two anisotropy profiles indicate the presence of several substructures in the halo.

We note that  $a_\phi(\theta)$  and  $a_\theta(\phi)$  are also sensitive to the choice of the number of bins. However, the locations of the spikes in the two anisotropy profiles do not depend on the choice of  $m_\theta$  and  $m_\phi$ . So the most anisotropic directions in the stellar halo can be correctly identified with any choice of  $m_\theta$  and  $m_\phi$ . The degree of anisotropy at each spike generally increases with the increasing number of bins ( $m_{total}$ ) for the same reasons mentioned earlier.

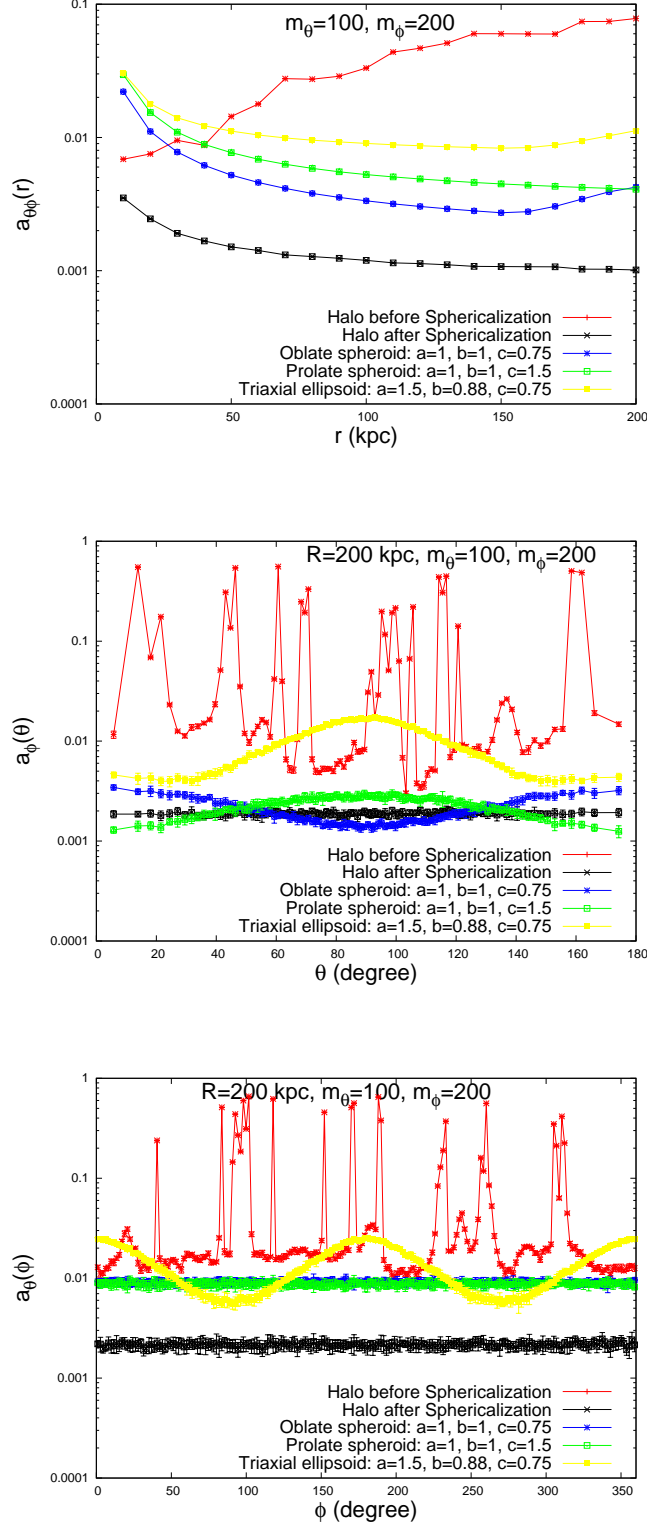


**Figure 3.** The top, middle and bottom panels of this figure respectively compares the whole-sky anisotropy, anisotropy at fixed polar angle and anisotropy at fixed azimuthal angle in Halo 1 before and after the sphericalization. The anisotropies in a set of mock halos with same density profile but different shapes are also compared in the same panels. The  $1 - \sigma$  error-bars at each data point are obtained from 10 jackknife samples for the original halo and their sphericalized versions. We use 10 independent realizations to obtain the  $1 - \sigma$  error-bars for the mock halos.

### 3.2 Comparison with sphericalized halos: shape versus substructures

The anisotropy in a stellar halo may arise from three different sources: the substructures, the shape and the discreteness noise in a stellar halo. We want to estimate their contributions to the anisotropy in a stellar halo. We carry out an analysis following the procedure outlined in [subsection 2.2](#).

We randomize the polar and azimuthal coordinates of each stellar particle within a given radius keeping their radial distances fixed. We refer to this process as sphericalization of the stellar halo. The sphericalized versions of the stellar halo would not contain any substructures. Further, all the information about the halo shape is also lost after the sphericalization. The sphericalized halos are expected to have the same radial density profile as the original stellar halo.

The sphericalization of a stellar halo is thus expected to remove all the anisotropies caused by the substructures and non-spherical shape of the halo. Consequently, we expect a significant reduction in the anisotropy of the stellar halo after its sphericalization. A small residual anisotropy would still be present in the halo after the sphericalization. This anisotropy is due to the Poisson noise that originates from the discrete nature of the distribution. We can compare the anisotropy in the original stellar halo and its sphericalized versions to extract important information about the substructures and shape of the halo.

The analysis in [subsection 3.1](#) shows that the anisotropies tend to converge at higher values of  $m_{total}$ . We set  $m_{\theta} = 100$  and  $m_{\phi} = 200$  as the default choice of binning for the rest of our analysis. This choice corresponds to an area of  $\frac{41,253}{20,000} \approx 2$  square degrees for each bin. We compare the whole-sky anisotropy in the original halo with its sphericalized versions in the top panel of [Figure 3](#). We observe a large reduction in the whole-sky anisotropy throughout the radius range. The non-zero whole-sky anisotropy in the sphericalized versions of the halo is caused by the Poisson noise. It decreases with the increasing radius of the halo. In contrast, the whole-sky anisotropy in the original halo rises with increasing radius. The ratio of anisotropies in the original and the sphericalized halos increases from 2 to 80 in the radius range 10 kpc to 200 kpc. The increase in amplitude of the ratio with radius indicates that the stellar halo becomes progressively more anisotropic at larger radii. We compare the whole-sky anisotropies in a set of smooth halos with different shapes in the same panel and find that the whole-sky anisotropies are significantly larger in these halos than the sphericalized versions of the original one. They even surpass the anisotropies in the original halo at a radius  $< 50$  kpc. However, the whole-sky anisotropies in oblate, prolate and triaxial halos are significantly smaller than the original halo at a radius beyond 50 kpc. It indicates that the whole-sky anisotropies at smaller and larger radii may be respectively determined by the shape and substructures of the halo.

In [Figure 3](#), we note that the anisotropies at fixed polar angle or fixed azimuthal angle in the original stellar halo have a smooth and an irregular component. The smooth and irregular components are not separately visible in the whole-sky anisotropies as it is calculated at each radius using all the solid angle bins. The irregular component originates from the substructures on smaller scales and is expected to disappear after the sphericalization. The smooth component of the anisotropy must remain unchanged after the sphericalization provided it originates from the discreteness noise alone. However, there could be an additional contribution to anisotropy from the non-spherical shape of the halo. We expect a reduction in the anisotropy of the smooth component if the shape of the halo contributes to the anisotropy at fixed polar angle and anisotropy at fixed azimuthal angle. We show these anisotropies inside Halo 1 in the middle and bottom panels of [Figure 3](#). In both the panels, we find a

significant reduction in the anisotropies after the sphericalization. The sphericalization of the halo completely eliminates the highly irregular component of the anisotropy. Furthermore, it also significantly depletes the approximately uniform component of the anisotropy in the original halo. The residual anisotropy in the halo after the sphericalization can only arise due to the discreteness noise. We find that the residual anisotropy in the sphericalized halos are  $\sim 4 - 5$  times smaller than the approximately uniform component of the anisotropy in the original halo. So the approximately uniform component of anisotropy in the original halo can not arise due to the discreteness noise alone. On the other hand, the fluctuating part of the anisotropy in the halo is  $\sim 200 - 300$  times larger than the residual anisotropy. It indicates that the substructures are the most dominant source of anisotropy in the stellar halo.

These results suggest that the substructures and the discreteness noise may not be the only sources of anisotropy in a stellar halo. The shape of the stellar halo may also significantly contribute to the anisotropy. We can quantify the contribution to the anisotropy from the halo shape. We compare the results from the original halo with a set of smooth halos with the same density profile ( $\sim r^{-3}$ ) but different shapes (subsection 2.3). We find that the non-spherical shape of a stellar halo can indeed introduce additional anisotropies in addition to the anisotropies due to the discreteness noise. We note that none of the three shapes considered here accurately describe the shape of the Halo 1. Nonetheless, our results indicate that the reduction in the approximately uniform component of anisotropy after sphericalization could be explained by the non-spherical shape of the halo. This distinction between the anisotropies may allow us to constrain the shape of the stellar halo as well as its substructure content.

The different orientations of the non-spherical halos would inevitably modulate the signals from the large-scale asymmetry present in the halo. We do not address the possible degeneracy between shape and orientation of the low-order ellipsoidal contribution in this work. We plan to address these issues in a future work.

### 3.3 Comparison of anisotropy in different stellar halos

We analyze all the 11 stellar halos from the Bullock & Johnston suite of simulations. The whole-sky anisotropy in these 11 stellar halos are compared with each other in Figure 4. The results suggest that the different stellar halos exhibit different degrees of whole-sky anisotropy at any given radius. The radial variation of the anisotropy is also different in each halo. The anisotropy plateaus out at different radii for each stellar halo. For instance, the whole-sky anisotropy increases up to 150 kpc in Halo 2, whereas it keeps increasing up to 270 kpc in Halo 1. Such differences in the anisotropy may arise from the diverse assembly history of the stellar halos. Despite such differences, nearly all the stellar halos have a tiny and similar anisotropy within a radius of 50 kpc from the centre. This re-emphasizes that all the stellar halos have a smoother core. The gradual increase of the anisotropy in the radially outward direction in all cases indicates an ‘inside out’ build-up of the stellar halo. The simulations used in this work assume hierarchical structure formation and the results of our analysis are qualitatively consistent with this assumption. A more detailed analysis is required to test the standard view of how mass is deposited in the stellar halo [84].

## 4 Conclusions

In this work, we analyze the anisotropy in a set of stellar halos from the Bullock & Johnston suite of simulations. Our main findings can be summarized as follows:

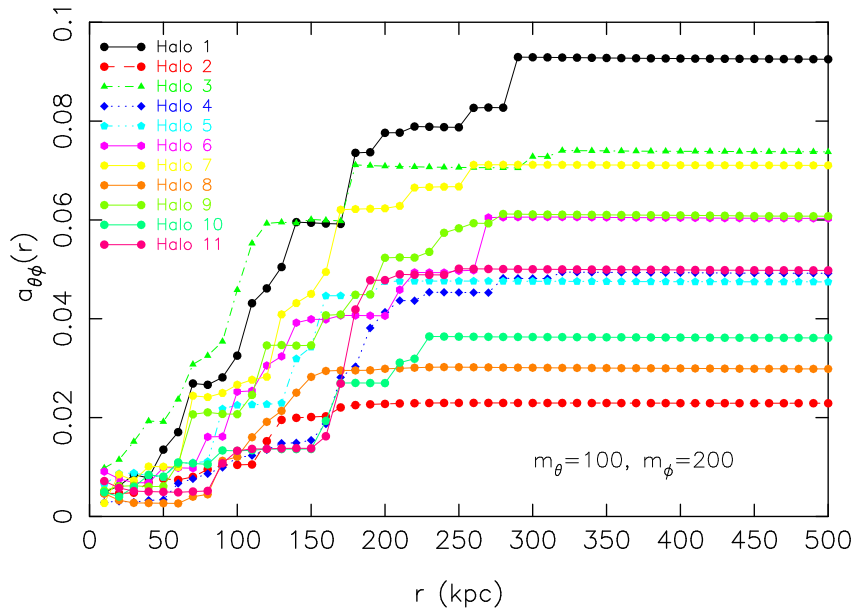


**Figure 4.** This figure compares the whole-sky anisotropy as a function of the distance from the centre of the halo for all the 11 halos in the Bullock & Johnston suite of simulations.

(i) All the stellar halos exhibit a very smooth structure within a radius of  $\sim 50$  kpc from their centres. The anisotropy in each halo increases with the radial distance from the centre and plateaus out beyond a certain radius. The halos are most anisotropic in their outer parts. The degree of anisotropy and its radial variation is different for each stellar halo suggesting a wide variety of assembly history. Such differences may provide useful constraints on the late-time accretion histories of galaxies. Our results indicate an inside out formation of stellar halo which is qualitatively consistent with the assumption of hierarchical structure formation in the simulations.

(ii) The anisotropies at fixed polar or azimuthal angle in a stellar halo show two distinct contributions. These anisotropies can be thought of as a superposition of a nearly constant part and a highly fluctuating part. The nearly constant part represents the anisotropy in the smooth component of the halo, whereas the fluctuating part corresponds to the anisotropy from its lumpy component. We sphericalize the stellar halos by randomizing the polar and azimuthal coordinates of all the stellar particles and keeping their radial coordinates fixed. This destroys all the substructures and hence eliminates the fluctuating part of the anisotropy. The approximately uniform component of the anisotropy should not be affected by the sphericalization if the anisotropy in the smooth component originates purely from the Poisson noise. However, we observe a reduction in the approximately uniform component of the anisotropy after the sphericalization, which suggests a non-spherical shape of the stellar halo. A non-spherical shape of the halo may introduce additional anisotropies in the distribution. Any information about the non-spherical shape of the original halo would be completely wiped

out after the sphericalization. We note that the reduction in the approximately uniform component of the anisotropy may be explained by considering different shapes of the stellar halo. It implies that the reduction in the approximately uniform component of the anisotropy is caused by the destruction of the shape of the halo, and the destruction of the substructures eliminates the fluctuating part. In other words, the anisotropy signal includes contributions from both the large-scale non-spherical shape of the halo and the small scale substructure, with the latter dominating separate the contributions to anisotropy from the shape and substructure.

We propose a statistical method to quantify the substructures and shape of the stellar halo. The limitations of the method are the following. The entropy depends on the choice of binning and the Poisson sampling rate. However, the relative character of the entropy does not pose any problem provided the distributions are compared with the same binning and sampling rate. Further, the existing observational datasets for galactic stellar halo do not provide a full sky coverage. One also needs to correct for the selection biases and the systematic present in the observational data before applying the proposed method to constrain the shape of the stellar halo and the substructures therein.

The shape of the stellar halo is usually determined directly by fitting prolate, oblate and triaxial smooth and broken power-law models [16, 20]. One can also infer the shape by analyzing the orbits of the stars and the dynamical modelling of the stellar halo [80, 81]. Our method is different from these traditional techniques. It is solely based on the measurement of anisotropies present in the halo. The method involves only a sphericalization of the stellar halo and a comparison of the anisotropies in the halo before and after the sphericalization.

The method is entirely based on the measurement of the spatial anisotropy. It does not require any dynamical modelling and the analysis of the stellar orbits. So the velocities of the stellar particles are not needed. It also does not require us to identify the individual substructures in the stellar halo. The method is relatively simple and can serve as an alternative and complementary technique for measuring shape of the stellar halo.

It would also be interesting to relate the anisotropy measurements with the stellar metallicity distribution and chemical abundance patterns of the halo. The distribution and abundance of the metals in the halo are crucial for understanding the chemical evolution of the galaxy [4]. The chemical evolution of the halo can be predicted in some models [82, 83] and can be also studied from observations. The old stellar population in the halo that formed earlier are known to be metal-poor [12, 82]. These metal-poor stars are the best tracers for the assembly history of the galaxy. They are usually found at larger distances from the centre of the halo. Contrary to this, the metal-rich stars are populated near the centre of the halo. Simulations suggest that the outer part of the stellar halo is primarily assembled from the less-massive satellites, which are most metal-poor due to the truncated star formation [84]. The existence of such a metallicity gradient in the stellar halo is studied in several works using simulations [85–87] and observations [88–90]. We want to explore the possible relations between the metallicity distributions and the anisotropy using simulated stellar halos in future works.

Our method can be also applied to the distribution of stars with a partial sky coverage. In future, we also plan to use our method to study the stellar halo of the Milky Way using observational data from SDSS [91] and Gaia [92].

## ACKNOWLEDGEMENT

I sincerely thank an anonymous reviewer for the detailed comments and valuable suggestions that helped me to significantly improve the presentation in the draft. The author acknowledges financial support from the SERB, DST, Government of India through the project CRG/2019/001110. BP would also like to acknowledge IUCAA, Pune, for providing support through the associateship programme.

## References

- [1] S. D. M. White, & M. J. Rees, *MNRAS*, **183**, 341 (1978)
- [2] P. J. E. Peebles, J. T. Yu, *ApJ*, **162**, 815 (1970)
- [3] W. H. Press, P. Schechter, *ApJ*, **187**, 425 (1974)
- [4] K. Freeman, J. Bland-Hawthorn, *ARA&A*, **40**, 487 (2002)
- [5] K. V. Johnston, L. Hernquist, M. Bolte, *ApJ*, **465**, 278 (1996)
- [6] A. Helmi, & S. D. M. White, *MNRAS*, **307**, 495 (1999)
- [7] J. S. Bullock, A. V. Kratsov, & D. H. Weinberg, *ApJ*, **548**, 33 (2001)
- [8] J. S. Bullock, & K. V. Johnston, *ApJ*, **635**, 931 (2005)
- [9] A. P. Cooper, S. Cole, C. S. Frenk, S. D. M. White, J. Helly, A. J. Benson, G. De Lucia, et al., *MNRAS*, **406**, 744 (2010)
- [10] A. S. Font, I. G. McCarthy, R. A. Crain, T. Theuns, J. Schaye, R. P. C. Wiersma, C. Dalla Vecchia, *MNRAS*, **416**, 2802 (2011)
- [11] A. Helmi, *A&ARv*, **15**, 145 (2008)
- [12] O. J. Eggen, D. Lynden-Bell, A. R. Sandage, *ApJ*, **136**, 748 (1962)
- [13] L. Searle, & R. Zinn, *ApJ*, **225**, 357 (1978)
- [14] B. Yanny, et al., *ApJ*, **540**, 825 (2000)
- [15] S. R. Majewski, M. F. Skrutskie, M. D. Weinberg, & J. C. Ostheimer, *ApJ*, **599**, 1082 (2003)
- [16] E. F. Bell, D. B. Zucker, V. Belokurov, S. Sharma, K. V. Johnston, J. S. Bullock, D. W. Hogg, et al., *ApJ*, **680**, 295 (2008)
- [17] E. F. Bell, X. X. Xue, H.-W. Rix, C. Ruhland, D. W. Hogg, *AJ*, **140**, 1850 (2010)
- [18] M. Jurić, et al., *ApJ*, **673**, 864 (2008)
- [19] R. De Propris, C. D. Harrison, P. J. Mares, *ApJ*, **719**, 1582 (2010)
- [20] A. J. Deason, V. Belokurov, N. W. Evans, *MNRAS*, **416**, 2903 (2011)
- [21] A. J. Deason, V. Belokurov, S. E. Koposov, C. M. Rockosi, *ApJ*, **787**, 30 (2014)
- [22] B. Sesar, M. Juric, Z. Ivezić, *ApJ*, **731**, 4 (2011)
- [23] C. T. Slater, E. F. Bell, E. F. Schlafly, et al., *ApJ*, **791**, 9 (2014)
- [24] C. T. Slater, D. L. Nidever, J. A. Munn, E. F. Bell, S. R. Majewski, *ApJ*, **832**, 206 (2016)
- [25] P. R. Kafle, S. Sharma, G. F. Lewis, J. Bland-Hawthorn J., *ApJ*, **794**, 59 (2014)
- [26] X.-X. Xue, H.-W. Rix, Z. Ma, H. Morrison, J. Bovy, B. Sesar, W. Janesh, *ApJ*, **809**, 144 (2015)
- [27] V. Belokurov, D. Erkal, N. W. Evans, S. E. Koposov, A. J. Deason, *MNRAS*, **478**, 611 (2018)

- [28] A. Helmi, C. Babusiaux, H. H. Koppelman, D. Massari, J. Veljanoski, A. G. A. Brown, *Nature*, **563**, 85 (2018)
- [29] H. Li, C. Du, S. Liu, T. Donlon, H. J. Newberg, *ApJ*, **874**, 74 (2019)
- [30] S. A. Bird, X.-X. Xue, C. Liu, J. Shen, C. Flynn, C. Yang, *AJ*, **157**, 104 (2019)
- [31] R. P. Naidu, C. Conroy, A. Bonaca, B. D. Johnson, Y.-S. Ting, N. Caldwell, D. Zaritsky, et al., *ApJ*, **901**, 48 (2020)
- [32] S. R. Majewski, *ARA&A*, **31**, 575 (1993)
- [33] M. Chiba, & T. C. Beers, *AJ*, **119**, 2843 (2000)
- [34] A. Helmi, S. D. M. White, *MNRAS*, **307**, 495 (1999)
- [35] C. J. Grillmair, *ApJ Letters*, **645**, L37 (2006)
- [36] V. Belokurov, N. W. Evans, M. J. Irwin, et al., *ApJ*, **658**, 337 (2007)
- [37] H. J. Newberg, B. A. Willett, B. Yanny, & Y. Xu, *ApJ*, **711**, 32 (2010)
- [38] R. A. Ibata, G. Gilmore, M. J. Irwin, *Nature*, **370**, 194 (1994)
- [39] Ž. Ivezić, J. Goldston, K. Finlator K., G. R. Knapp, B. Yanny, T. A. McKay, S. Amrose, et al., *AJ*, **120**, 963 (2000)
- [40] B. Yanny, et al., *ApJ*, **588**, 824 (2003)
- [41] R. A. Ibata, M. J. Irwin, G. F. Lewis, A. M. N. Ferguson, & N. Tanvir, *MNRAS*, **340**, L21 (2003)
- [42] S. Duffau, R. Zinn, A. K. Vivas, G. Carraro, R. A. Méndez, R. Winnick, & C. Gallart, *ApJ*, **636**, L97 (2006)
- [43] V. Belokurov, et al., *ApJ*, **657**, L89 (2007)
- [44] L. L. Watkins, et al., *MNRAS*, **398**, 1757 (2009)
- [45] R. Ibata, M. Irwin, G. Lewis, A. M. N. Ferguson, & N. Tanvir, *Nature*, **412**, 49 (2001)
- [46] A. M. N. Ferguson, M. J. Irwin, R. A. Ibata, G. F. Lewis, & N. R. Tanvir, *AJ*, **124**, 1452 (2002)
- [47] D. B. Zucker, et al., *ApJ*, **612**, L117 (2004)
- [48] R. A. Ibata, et al., *ApJ*, **671**, 1591 (2007)
- [49] A. W. McConnachie, M. J. Irwin, R. A. Ibata, J. Dubinski, L. M. Widrow, N. F. Martin, P. Côté, et al., *Nature*, **461**, 66 (2009)
- [50] Z. Shang, et al., *ApJ*, **504**, L23 (1998)
- [51] D. Martínez-Delgado, R. J. Gabany, K. Crawford, S. Zibetti, S. R. Majewski, H.-W. Rix, J. Fliri, et al., *AJ*, **140**, 962 (2010)
- [52] M. Mouhcine, R. Ibata, & M. Rejkuba, *ApJ*, **714**, L12 (2010)
- [53] M. G. Abadi, J. F. Navarro, & M. Steinmetz, *MNRAS*, **365**, 747 (2006)
- [54] G. De Lucia, & A. Helmi, *MNRAS*, **391**, 14 (2008)
- [55] V. Springel, J. Wang, M. Vogelsberger, A. Ludlow, A. Jenkins, A. Helmi, J. F. Navarro, et al., *MNRAS*, **391**, 1685 (2008)
- [56] A. Monachesi, F. A. Gómez, R. J. J. Grand, C. M. Simpson, G. Kauffmann, S. Bustamante, F. Marinacci, et al., *MNRAS*, **485**, 2589 (2019)
- [57] A. S. Font, I. G. McCarthy, R. Poole-Mckenzie, S. G. Stafford, S. T. Brown, J. Schaye, R. A. Crain, et al., *MNRAS*, **498**, 1765 (2020)

- [58] A. Helmi, A. P. Cooper, S. D. M. White, S. Cole, C. S. Frenk, J. F. Navarro, *ApJL*, **733**, L7 (2011)
- [59] A. Zolotov, B. Willman, A. M. Brooks, F. Governato, C. B. Brook, D. W. Hogg, T. Quinn, et al., *ApJ*, **702**, 1058 (2009)
- [60] C. W. Purcell, J. S. Bullock, S. Kazantzidis, *MNRAS*, **404**, 1711 (2010)
- [61] G. Iorio, V. Belokurov, *MNRAS*, **482**, 3868 (2019)
- [62] S. Tremaine, J. P. Ostriker, *MNRAS*, **306**, 662 (1999)
- [63] A. J. Deason, R. P. Van der Marel, P. Guhathakurta, S. T. Sohn, T. M. Brown, *ApJ*, **766**, 24 (2013)
- [64] D. Nelson, V. Springel, A. Pillepich, V. Rodriguez-Gomez, P. Torrey, S. Genel, M. Vogelsberger M., et al., *Computational Astrophysics and Cosmology*, **6**, 2 (2019)
- [65] W. Wu, G. Zhao, X.-X. Xue, W. Pei, C. Yang, Accepted by *AJ*, arXiv, arXiv:2205.14815 (2022)
- [66] M. P. Rey, T. K. Starkenburg, *MNRAS*, **510**, 4208 (2022)
- [67] J. J. Han, R. P. Naidu, C. Conroy, A. Bonaca, D. Zaritsky, N. Caldwell, P. Cargile, et al., *ApJ*, **934**, 14 (2022)
- [68] X.-X. Xue, H.-W. Rix, B. Yanny, T. C. Beers, E. F. Bell, G. Zhao, J. S. Bullock, et al., *ApJ*, **738**, 79 (2011)
- [69] R. P. Naidu, C. Conroy, A. Bonaca, B. D. Johnson, Y.-S. Ting, N. Caldwell, D. Zaritsky, et al., *ApJ*, **901**, 48 (2020)
- [70] L. M. Elias, L. V. Sales, P. Creasey, M. C. Cooper, J. S. Bullock, R. M. Rich, L. Hernquist, *MNRAS*, **479**, 4004 (2018)
- [71] A. R. Zentner, A. V. Kravtsov, O. Y. Gnedin, A. A. Klypin, *ApJ*, **629**, 219 (2005)
- [72] N. Mandelker, P. G. van Dokkum, J. P. Brodie, F. C. van den Bosch, D. Ceverino, *ApJ*, **861**, 148 (2018)
- [73] B. Pandey, *MNRAS*, **462**, 1630 (2016)
- [74] B. Pandey, *MNRAS*, **468**, 1953 (2017)
- [75] B. Pandey, *MNRAS*, **469**, 1861 (2017)
- [76] S. Sarkar, B. Pandey, R. Khatri, *MNRAS*, **483**, 2453 (2019)
- [77] B. Pandey, *MNRAS*, **430**, 3376 (2013)
- [78] C. E. Shannon, *Bell System Technical Journal*, **27**, 379 (1948)
- [79] B. Pandey, *MNRAS*, **463**, 4239 (2016)
- [80] J. Bovy, A. Bahmanyar, T. K. Fritz, N. Kallivayalil, *ApJ*, **833**, 31 (2016)
- [81] G. Sato, M. Chiba, *ApJ*, **927**, 145 (2022)
- [82] B. Robertson, J. S. Bullock, A. S. Font, K. V. Johnston, L. Hernquist, *ApJ*, **632**, 872 (2005)
- [83] A. S. Font, K. V. Johnston, J. S. Bullock, B. E. Robertson, *ApJ*, **646**, 886 (2006)
- [84] N. C. Amorisco, *MNRAS*, **464**, 2882 (2017)
- [85] E. Starkenburg, K. A. Oman, J. F. Navarro, et al., *MNRAS*, **465**, 2212 (2017)
- [86] S. Salvadori, A. Ferrara, R. Schneider, E. Scannapieco, & D. Kawata, *MNRAS*, **401**, L5 (2010)
- [87] P. B. Tissera, T. C. Beers, D. Carollo, & C. Scannapieco, *MNRAS*, **439**, 3128 (2014)
- [88] E. Fernandez-Alvar, C. Allende Prieto, K. J. Schlesinger, et al., *A&A*, **577**, A81 (2015)

- [89] T. C. Beers, Y. K. Kim, et al., *ApJ*, **836**, 91 (2017)
- [90] S. E. Dietz, J. Yoon, T. C. Beers, V. M. Placco, *ApJ*, **894**, 34 (2020)
- [91] D. G. York, et al., *AJ*, **120**, 1579 (2000)
- [92] Gaia Collaboration, T. Prusti, J. H. J. de Bruijne, A. G. A. Brown, A. Vallenari, C. Babusiaux, C. A. L. Bailer-Jones, et al., *A&A*, **595**, A1 (2016)